PCCP

Accepted Manuscript

ROYAL SOCIETY OF CHEMISTRY

www.rsc.org/pccp

Analysis of Heterogeneous Uptake by Nanoparticles via Differential Mobility Analysis-Drift Tube Ion Mobility Spectrometry

Derek R. Oberreit, Peter H. McMurry, & Christopher J. Hogan Jr.*

Department of Mechanical Engineering, University of Minnesota, 111 Church St. S.E., Minneapolis, MN, 55455, USA

Submitted To:

Physical Chemistry Chemical Physics

***To whom correspondence should be addressed: hogan108@umn.edu, Tel: 1-612-626-8312, Fax: 1-612-625-6069**

ABSTRACT

Improved methods are needed to study sorption of vapor molecules by particles in the gas phase (heterogeneous uptake), which is an important process in both natural and engineered environments. Here, a new measurement system, composed of a differential mobility analyzer (DMA) and drift tube ion mobility spectrometer (DTIMS) in series, is used to examine the heterogeneous uptake of water vapor by 2.85-7.6 nm particles composed of lithium and sodium iodide. The extent of heterogeneous uptake is determined by controlling the relative humidity of the drift region in DTIMS in the 0 - 30% range (in air at atmospheric pressure and room temperature), and is quantified via the dimensionless growth factor (GF), i.e. the ratio of the mobility diameter of particles at a prescribed relative humidity relative to their mobility diameter under dry conditions. The precision in GF estimation of the DMA-DTIMS system is shown to be below 0.2%. An analytical equation to calculate the growth factor, based upon predictions of the equilibrium constants for the successive uptake of vapor molecules by particles, is also presented. While the equation is sufficiently general to enable comparison between measured GFs and predictions from any theoretical expression for equilibrium constants, we specifically compare measurements to GF predictions based on the classical Kelvin-Thomson-Raoult (KTR) model for the vapor pressure of a small particle, with consideration of the influence of the ion-dipole potential on water vapor-nanoparticle collisions. It is shown that KTR calculations drastically underpredict the extent of heterogeneous uptake for the examined nanoparticles.

INTRODUCTION

Nanoparticle-vapor molecule collisions lead to the sorption of vapor molecules onto nanoparticles (heterogeneous uptake), and thus vapor molecules present in an aerosol can substantially alter particle size and chemical composition.[1-4] Classical relationships are frequently invoked to predict the extent of heterogeneous uptake, which are based upon the Kelvin-Thomson equation[5, 6] and invoke bulk property values for both vapor molecules and particles. However, in many situations such classical relationships are inadequate;[7-10] errors with classical approaches manifest when modeling heterogeneous uptake by particles which have sizes close to molecular dimensions,[7, 8] when the particle is soluble in the condensed liquid,[11-13] or if sorption leads to formation of a vapor molecule monolayer on the particle surface.[14] Most notably, the fraction of nanometer scale particles which grow into micrometer sized droplets via heterogeneous uptake when exposed to supersaturated vapor (i.e. as in condensation particle counters) is found to be strongly dependent on particle material and charge state in a manner not explained by classical relationships.[15, 16] While modifications to classical approaches have been developed to address these issues,[13, 17-22] measurements of vapor molecule sorption by aerosol particles remain necessary to better understand heterogeneous uptake, particularly during the initial stages of uptake by sub-10 nm particles, i.e. when the sorbed species represents only a small fraction of the total particle mass and in a size range where classical relationships have yielded poor agreement with measurements.

The experimental techniques which have been used to study such uptake can be described as either equilibrium or non-equilibrium methods. Although the latter[7, 10, 23, 24] provide valuable information on particle growth in supersaturated environments, measurements on particles are made only after uptake increases particle sizes to the supermicrometer size range. Therefore,

these methods do not afford direct examination of the initial stages of uptake. Conversely, techniques that investigate heterogeneous uptake under equilibrium conditions, including tandem differential mobility analysis (TDMA),[25, 26] electrodynamic balance (EDB) measurements,[27-30] and high pressure mass spectrometry (HPMS)[8, 9], can be used to examine finite degrees of heterogeneous uptake and hence the initial stages of growth. Collectively, use of these approaches enables study of heterogeneous uptake onto particles over a wide size range, yet leaves a window in the ~2 - 10 nm size (diameter) range where measurements are difficult. HPMS is best suited for subnanometer molecular clusters, while TDMAs typically perform best above ~7 nm[20] (though smaller particles have been examined[31]). EDB systems are limited to submicrometer and larger particles (which can be observed optically).

The objective of this work is therefore to develop and demonstrate the capabilities of a measurement system for equilibrium measurements of heterogeneous uptake by sub-10 nm particles. The measurement system is composed of a high sheath flow rate DMA coupled to a recently developed[32] drift tube ion mobility spectrometer (DTIMS), unique from most DTIMS instruments[33] in that it is interfaced with an aspirating condensation particle counter (CPC). The use of a DMA-DTIMS aids in overcoming long counting times encountered using TDMA with low concentrations of particles in the sub 10 nm size range. In the proceeding sections, the DMA-DTIMS system is described in detail and laboratory results for the sorption of water vapor molecules to 2.85 – 7.6 nm LiI and NaI salt particles are presented. An analysis approach is provided which facilitates comparison of DMA-DTIMS measurements to theoretical predictions of heterogeneous uptake.

EXPERIMENTAL METHODS

DMA-DTIMS System Description

A schematic of the DMA-DTIMS system is shown in Figure 1a. The aerosol particles under examination are first sampled into a DMA, which transmits only charged particles with a narrow range of electrical mobilities centered about a value Z_p, adjustable by varying the DMA operating conditions (sheath flowrate and voltage difference between electrodes). The DMA in the presented system is the ½ mini-DMA (Nanoengineering Corp.), which is described in detail by Fernandez de la Mora & Kozlowski,[34] with the working principles of modest-to-high resolving power DMAs also described elsewhere.[35] The DMA is operated with a sheath flow of air in recirculating mode (using a Domel Inc. vacuum blower). A water cooled heat exchanger, similar to that used by Fernandez-Garcia & Fernandez de la Mora,[36] is used to maintain the sheath gas temperature at ~22^o C. The flowrate of aerosol entering and exiting the DMA is set to ~5 l min^{-1}.

Because the sheath flowrate is on the order of 100 l min^{-1}, it is difficult to measure precisely. The DMA electrical mobility-voltage relationship is instead inferred through measurement of an ion of known electrical mobility; with the transmission of an ion of electrical mobility Z_{cal} at applied voltage V_{cal}, the electrical mobility Z_p of a charged particle maximally transmitted at applied voltage V is given by the relationship: $Z_p = (V_{cal}/V)Z_{cal}$ (with constant DMA sheath flowrate). In calibration we use the tetradodecylammonium$^+$ ion, whose electrical mobility was measured accurately by Ude & Fernandez de la Mora[37] in air, near atmospheric pressure close to 20^o C. Assuming that a hard-sphere relationship can describe the electrical mobility of this ion (supported by measurements[38] and calculations[39] by Larriba & coworkers), the measured tetradodecylammonium$^+$ electrical mobility is adjusted[40] to correct for the slight

temperature (23-24°C) and pressure (1% above atmospheric pressure) differences between Ude & Fernandez de la Mora's experiments and those presented here.

For safety reasons, voltage is applied to the inner electrode of the DMA while the outer electrode is held at ground potential. Particles migrate from the outer electrode to the inner electrode, where the DMA outlet is located. A semiconductive polymeric tube (Ensital SD, Piper Plastics Inc., Illinois, USA) is connected to the outlet to isolate the DMA inner electrode electrostatically from the remainder of the measurement system. After exiting the DMA, the flow of electrical mobility selected particles is split; 1 l min^{-1} enters the DTIMS, while the remainder enters a HEPA filter and is vented to atmosphere. Like the DMA, the DTIMS separates charged particles from one another by their electrical mobilities, though in the DTIMS charged particles are driven by an electric field axially through a cylindrical drift region to a detector (a CPC). Therefore, all particles in a wide electrical mobility range are transmitted and travel along similar trajectories, but their arrival times at the detector depend on electrical mobility.[41]

The DTIMS is operated as described previously,[32] with 1 or 3 kV applied as the drift voltage and with a WCPC[42, 43] (water CPC) model 3788 (TSI Inc., Minnesota, USA) used as the detector. The WCPC operates with a flowrate of 0.615 l min^{-1}, and the DTIMS counter-flowrate is nominally set at 0.2 l min^{-1}, with the sum of these flows entering the drift region at the counterflow inlet. DTIMS measurements are quantified by arrival time distributions (ATDs), which express the number of particles detected per unit arrival time (or per unit log arrival time), as a function of the arrival time. The arrival time (t) is linked to the electrical mobility of a detected particle via a previously developed[32] dimensionless calibration equation:

$$\tau = 1.127\frac{Pe}{\Psi e} + .0047 \qquad (1a)$$

where τ is the dimensionless drift time, equivalent to tu_cL^{-1} (u_c is the average counterflow velocity; L is the drift region length), and Pe/Ψe is the ratio of the Peclet number to the dimensionless ratio of the electrostatic potential and the thermal energy (equivalent to $u_cLZ_p^{-1}V_D^{-1}$, where V_D is the applied voltage to the DTIMS).[32] This equation can be rearranged to express the inverse electrical mobility as:

$$Z_p = \left(0.887\frac{tV_D}{L^2} - 0.0041\frac{V_D}{u_cL^2}\right)^{-1} \quad (1b)$$

Total measurement times less than 10 seconds are employed. To control the vapor molecule concentration in the drift region, a nebulizer, depicted in Figure 1b, is placed upstream of the counterflow inlet. The nebulizer is operated with 0.815 l min^{-1} of ultra-high purity zero air (Airgas) with controlled water volumetric flow (using New Era syringe pump). Liquid water flowrates range from 0.05 – 4 μl min^{-1}. The present study is limited to measurements with water vapor in the RH < 30% range near room temperature. To remove residue particles remaining after the nebulizer (water droplets evaporate, however each droplet contains some amount of non-volatile residue) a glass fiber filter is placed downstream of the nebulizer prior to the counterflow inlet. The dew point of the drift region is nominally calculated from the mass flow rate of water entering the nebulizer and the counterflow inlet flowrate (0.815 l min^{-1}), and periodically validated using a dew point hygrometer (General Eastern). It is found that the measured and the calculated dew points differ by 0.5° C at most for the dew points that can be measured by the hygrometer. The temperature is also measured at the counterflow inlet, and used in conjunction with the dew point measurement/calculation to determine the RH of the drift region.

All DTIMS flows are maintained with mass flow controllers (MKS Instruments) and calibrated using a bubble-type flowmeter (Sensidyne Inc.). The operation of the complete DMA-

DTIMS system is controlled via a *Labview*^{TM} (National Instruments) program, and all voltages are applied using Bertan high voltage power supplies. Positively charged particles are examined for the presented results; thus, a negative voltage is applied to the DMA inner electrode and the drift voltage is positive. DTIMS ATDs are determined directly from the WCPC counts (collected via the *Labview*^{TM} program) and binned in units of log scale time.

Heterogeneous Uptake Analysis

As the examined particles are approximately spherical and singly charged (as explained subsequently), their diameters (d_p) can be estimated from their electrical mobilities via the free molecular limit of the Stokes-Millikan relationship[38]:

$$Z_p = \sqrt{\frac{\pi m_{air}}{8 k_B T}} \frac{3e}{\pi \rho \xi} \frac{1}{\left(d_p + d_{air}\right)^2} \quad (2)$$

where m_{air} and d_{air} are the average mass (29 Da) and diameter (0.3 nm) of the surrounding gas molecules, ρ is the gas mass density, ξ is a scattering coefficient (1.36), e is the unit charge, k_B is Boltzmann's constant and T is the temperature. In instances where the counterflow of the DTIMS is not humidified, the electrical mobility selected by the DMA and that corresponding to the peak arrival time (t_0) are identical ($Z_{p,0}$), and the diameter inferred from equation (2) corresponds to the dry particle diameter, d_0. However, with the counterflow humidified, heterogeneous uptake leads to particle growth and decreasing electrical mobilities. Provided the particles under examination are of identical chemical composition to one another, and particles reside in the drift region for times substantially longer than the system equilibration time, the extent of heterogeneous uptake can be quantified by calculating the dimensionless growth factor (GF)[12, 44]:

$$(GF)_{RH} = \frac{(d_p + d_{air})_{RH}}{d_0 + d_{air}} \quad (3)$$

where the subscript "*RH*" denotes the relative humidity in question, and $(d_p+d_{air})_{RH}$ is inferred from the peak arrival time in ATDs measured at counterflow relative humidity "*RH*" (with corresponding electrical mobility $Z_{p,RH}$). In using equations (2) and (3), we have not corrected for the change in gas properties brought about by the change in drift region gas composition when water vapor is added. At the highest relative humidities employed (22%), approximately 0.7% of the gas molecules in the drift region are water. In the absence of any heterogeneous uptake, noting that the addition of water vapor leads to a 0.25% decrease in both the gas density and effective molecular weight of air, equation (2) predicts that the particle electrical mobilities would increase by 0.1% due to the presence of water vapor. Shown subsequently, this is less than the uncertainty of growth factor measurements themselves (unless a large number of particles are counted) and further would lead to a growth factor below unity, i.e. the addition of water vapor alone would not decrease the electrical mobility of particles. However, with higher relative humidities and with small extents of heterogeneous uptake, the influence of water vapor on the background gas properties should be considered.

Aside from the influence of water vapor on background back properties, the finite resolution of the DT-IMS spreads out measured signal across the ATD, which reduces the precision with which the actual peak measurement time can be determined in a manner governed by Poisson (counting) statistics. To explore the influence of counting statistics on DMA-DTIMS measurements, we determine the standard deviation of the peak arrival time (σ_t) in measurements, following an analogous approach to the that utilized by Rader and McMurry[25] to examine the precision of TDMA systems. Specifically, we generate random data sets intended to mimic DMA-DTIMS results by approximating ATDs as Gaussian distributions with normalized

full width half maxima of 1/5, based upon the resolving power of the DTIMS[32] (and neglecting signal smearing by the DMA, which has a resolving power in excess of 25). For each distribution, ΔN_{peak}, the number of counts in the measurement channel corresponding to the peak arrival time, is selected in the range 10-1000. Additionally, the peak arrival time is varied from 1.5-3.5s, the total measurement time is assumed to be 5.0 s, and both 150 and 240 time channels (starting at 0.1 s) are used. To determine the number of counts (ΔN) in each time channel, artificial "noise" signal is input into simulated distributions by adding to each of the Gaussian time bin counts (ΔN_{Gaus}) the product of the Poisson standard deviation $(\Delta N_{Gaus})^{1/2}$ and a normally distributed random number of mean zero and unit standard deviation. Subsequently, peak arrival times are inferred by fitting a Gaussian curve to each ATD using least squares regression,[45] in which the contribution to the least squares error for each channel is weighted by $\Delta N^{1/2}$ within the channel. In fitting, only arrival times within two standard deviations of the peak drift time are considered. Finally, σ_t is calculated over 100 simulated ATDs for each prescribed value of ΔN_{peak}, the number of measurement channels, and true peak arrival time.

Figure 2 displays values of σ_t/t (where t is the specified peak arrival time) as a function of $\Delta N_{peak}/\Delta log_{10}(t)$ (where $\Delta log_{10}(t)$ is the log-scale channel width), which reveals that all simulated results collapse to a single curve, a power law regression to which gives: $\sigma_t/t = 0.6806\,[\Delta N_{peak}/\Delta log_{10}(t)]^{-0.545}$ ($R^2 = 0.9949$). To directly assess the influence of instrument precision on GF measurements, we define the standard deviation of the growth factor, σ_{GF}, as:

$$\sigma_{GF} = \left(\left[\sigma_{Zp^{-1},RH} \frac{dGF}{dZ^{-1}_{p,RH}} \right]^2 + \left[\sigma_{Zp^{-1},0} \frac{dGF}{dZ^{-1}_{p,0}} \right]^2 \right)^{1/2} \quad (4a)$$

where $\left(\frac{dGF}{dZ_{p,RH}^{-1}}\right)^2 = \frac{Z_{p,0}Z_{p,RH}}{4}$ and $\left(\frac{dGF}{dZ_{p,0}^{-1}}\right)^2 = \frac{Z_{p,0}^3}{4Z_{p,RH}}$. For the evaluation of dZ_p^{-1} terms, in most experiments it is acceptable to assume that random errors negligibly impact measured GFs when compared to errors due to counting statistics. The standard deviation of Zp^{-1} is defined as:

$$\sigma_{Zp^{-1}} = \frac{\partial Zp^{-1}}{\partial t}\sigma_t \qquad (4b)$$

which, when combined with equation (1b) gives:

$$\sigma_{Zp^{-1}} = \frac{V}{1.127L^2}\sigma_t \qquad (4c)$$

With the assumption that $\Delta N/\Delta log_{10}(t)$ at the peak arrival time is equivalent for measurements under both dry and humidified conditions, by combining equations (1b), (4a), & (4c), it is shown that:

$$\frac{\sigma_{GF}}{GF} = \frac{1}{1-0.0047\frac{L}{u_c t_{RH}}}\left(\frac{\sigma_{t,RH}}{2t_{RH}}\left(1+\left(\frac{t_0}{t_{RH}}\right)^2 GF^4\right)^{1/2}\right) \qquad (4d)$$

For a drift tube with extremely high counterflow velocity (or with a faster response detector, for which the time-independent term in equation 1a is negligible), combining equations (1b), (2), (3), & (4d) leads to:

$$\frac{\sigma_{GF}}{GF} = \frac{\sigma_{t,RH}}{2^{1/2}t_{RH}} \qquad u_c >> L/t_{RH} \qquad (4e)$$

Using equation (4d) and parameters corresponding to the present DMA-DTIMS system, Figure 2 additionally shows calculated values of σ_{GF}/GF for GF values of 1.0, 1.1, and 2.0, with t_0 held constant at 2.5s. For the measurements performed here, the mean σ_{GF}/GF was 0.0024 (with a standard deviation of 0.00045). Therefore, under the conditions operated, the DMA-DTIMS system had sufficient precision to distinguish measured GFs from classical predictions, with

greater precision achievable via measurement of larger numbers of particles. Additionally, the DMA-DTIMS combination has sufficient precision to quantify GFs only several percent above unity in the sub-10 nm particle size range, which has not been demonstrated with previously developed tandem mobility analysis systems.

Laboratory Measurements

With the DMA-DTIMS operated with the setting noted in the "*DMA-DTIMS System Description"* section, measurements of vapor uptake were performed for particles composed of lithium and sodium iodide. These salts were chosen for analysis due to their low saturated aqueous solution activities, $a_{w,sat}$, (0.186 ± 0.002 and 0.397 ± 0.006 at 20°C for LiI and NaI respectively).[46] Nanometer scale particles were generated via charge reduction electrospray with a model 3480 electrospray aerosol generator[47] (TSI Inc., Minnesota, USA) operated with a 40 μm inner diameter silica capillary and with ultrapure zero air as the carrier flow at 1.0 l min^{-1}. The electrosprayed solutions were prepared with HPLC grade methanol (Sigma-Aldrich, Saint Louis, MO, USA) at salt concentrations of 0.1, 0.3, and 1.0 mM. Ammonium acetate (20 mM) was added to increase the solution electrical conductivity, facilitating stable cone-jet formation. Although the addition of ammonium acetate led to significantly more NH_4^+, CH_3COO^- ions in electrospray solutions and generated droplets than Li^+, Na^+ or I^- ions, we believe this minimally influenced the chemical composition of electrospray generated particles, as ammonium acetate clusters themselves are known to be extremely volatile at room temperature (with cations and anions reacting and evaporating as ammonia and acetic acid, respectively). In separate differential mobility analyzer-mass spectrometer (DMA-MS) measurements (using the system described by Rus et al)[48] of electrosprayed ions generated from the solutions used in

experiments, we did not detect any stable NH_4^+ or CH_3COO^- containing cluster ions, while at non-volatile species concentrations of 20 mM under near-identical electrospray conditions, 1-10 nm diameter cluster ions are routinely observed.[38, 40, 49] Moreover, small perturbations to the chemical composition of the generated particles neither invalidate the ability of DMA-DTIMS system to detect heterogeneous uptake derived mobility shifts, nor do they strongly influence the results of the comparison performed to classical theory predictions.

A 5mCi Po-210 source was used to produce roughly equal concentrations of positive and negative ions, which, via collisions,[50, 51] reduced the charge level on droplets such that most of them did not fission during the evaporation process. The resulting size distribution of nanoparticles produced hence reflected the initial size distribution of the electrosprayed droplets (determined by the droplet size distribution and non-volatile salt volume fraction in the solutions used[52]). Upon achieving a near-steady state charge distribution due to collisions with ions, the majority of generated nanoparticles were neutral, and the majority of the charged particles were singly charged (positively or negatively).[51] In stable operation the electrospray aerosol generator produced particles in the 2-10 nm diameter range with a fairly monodisperse (geometric standard deviation of ~1.1) size distribution function, the geometric mean of which was adjustable based on the salt concentration in solution and liquid flowrate. An additional ~4.0 L min^{-1} was added immediately downstream of the EAG to reduce diffusion losses in the tubing leading to the DMA inlet. For each of the salt concentrations, the peak electrical mobility of the distribution was measured and this mobility was then selected by the DMA. DMA selected particles entered the DTIMS, operated with a prescribed RH. Between three and ten individual ATDs were accumulated for each DMA selected electrical mobility and RH value; reported ATDs are the average of these individual ATDs. A two-minute pause between different RH values was used to

ensure that RH within the drift tube achieved the prescribed value. After the final RH measurement the syringe pump was stopped and a final 'dry' ATD was measured after a ten-minute delay.

RESULTS AND DISCUSSION

Measurement Results

Figures 3 displays plots of the normalized, $\log_{10}$-based ATDs, i.e. the average normalized particle counts per unit of $\log_{10}$ arrival time ($\Delta N/\Delta log_{10}(t)/N_{tot}$, where N_{tot} is the total number of counts in all channels) as a function of arrival time, for DMA selected particles. The electrical mobilities (Z_p) of these particles (singly charged) are determined directly from the DTIMS calibration equation[32] and are also displayed in Figure 3 plots. Diameters corresponding to the peak electrical mobility selected by the DMA, calculated with equation (2), are labeled in each Figure 3 graph (i.e. the diameters of the particles at zero relative humidity). In the plot for initially 5.6nm NaI particles, a portion of the distribution was not measured, and therefore N_{tot} is artificially low. Apparent for measurements of both NaI and LiI particles is a shift in the peak arrival time in ATDs at higher drift region RHs, which is indicative of heterogeneous water uptake. To determine growth factors at each RH, the peak arrival time in each ATD is inferred by repeating the Gaussian fitting procedure noted previously in determining the DTIMS precision. The resulting growth factors are plotted as a function of RH for three selected diameters of lithium iodide and sodium iodide clusters in Figures 4a and 4b respectively. The errors bars in these plots are calculated with equation (4d) using measurement results. A growth factor slightly less than unity is found at lower RHs in several instances. This is possibly due to either restructuring particles facilitated by collisions with water vapor molecules, or evaporation

of ammonium acetate upon the addition of water, as it is beyond what is expected due to the change in background gas properties upon introduction of water vapor. Such restructuring upon interaction with trace amounts of water vapor has been observed for sodium chloride nanoparticle generated in furnace reactors,[12] however, further examination of the structures of electrospray generated iodide salt nanoparticles would be necessary to determine whether this is a possibility in the present study. For lithium iodide, higher GFs are observed for larger particles, and the onset of growth for larger particles also occurs at lower RH values. For sodium iodide particles, larger GFs are again observed for the larger particles examined at the highest RHs; however, unlike lithium iodide particles, the onset of growth is apparent at lower RHs for the smaller particles examined.

Comparison to Theoretical Predictions

The presented results show that DMA-DTIMS measurements can be used to probe heterogeneous uptake onto nanometer scale particles. Furthermore, measurements reveal differences in particle growth factors for different particle chemical properties and dry particle diameters. We now show how the extent of heterogeneous uptake observed, quantified in terms of the growth factor, can be compared to theoretical predictions, and specifically compare to predictions based on classical relationships. For this analysis, we consider monomobile, singly charged nanoparticles of homogenous chemical composition, which uptake individual vapor molecules. We further assume that nanoparticles traversing the drift region are in equilibrium with the surrounding water vapor, such that the rate of vapor molecule sorption onto nanoparticles with *g-1* vapor molecules attached (i.e. the number of vapor molecule- nanoparticle collisions per unit volume per unit time) is equivalent the rate of desorption of vapor molecules

from nanoparticles with g vapor molecules attached. This assumption is reasonable, given the short timescales for vapor molecule-particle collisions relative to particle drift times in the DTIMS. Therefore, the relationship:

$$\frac{n_g}{n_{g-1}} = K'_{eq,g} = K_{eq,g} n_{sat} S = \frac{\alpha_{g-1}}{\beta_g} \quad (5a)$$

holds valid, where n denotes a number concentration, $K'_{eq,g}$ denotes the dimensionless equilibrium constant for the reaction $n_{g-1} \rightleftharpoons n_g$ (i.e. modeling the reaction as a reversible unimolecular reaction), $K_{eq,g}$ is the dimensional equilibrium constant, n_{sat} is the vapor molecule concentration at saturation, S is the saturation ratio ($S = RH/100$), α_{g-1} is the sorption rate coefficient (vapor molecules sorbed per unit time from a single nanoparticle) and β_g is the desorption rate coefficient (vapor molecules desorbed per unit time from a single nanoparticle).

The sorption rate is dependent upon the vapor molecule concentration ($n_{sat}S$), the sticking probability (assumed unity here), as well as the vapor molecule-nanoparticle collision kernel.[53, 54] For nanoparticles in the 2.85-7.6 nm diameter range, the ion-dipole potential between charged nanoparticles and water vapor molecules (dipole moment = 1.85 D) may influence vapor molecule motion[55]. We therefore calculate α_{g-1} with the relationship:

$$\alpha_{g-1} = \frac{n_{sat} S \mathrm{H_S} k_B T \left(d_{g-1} + d_v\right)^3}{8 m_v D_v} \frac{\eta_{FM}^2}{\eta_C} \quad (5b)$$

where $\mathrm{H_S}$ is the dimensionless collision rate coefficient/collision kernel,[53, 55] d_{g-1} is the diameter of the particle undergoing vapor molecule collisions (with *g-1* vapor molecules sorbed), d_v is the effective vapor molecule diameter (~0.38 nm, approximated from water's bulk density and molecular weight), m_v is the mass of the vapor molecule, D_v is the diffusion coefficient of the vapor in the background gas, and η_{FM} and η_C are the free molecular and continuum enhancement

factors brought about by potential interactions, respectively.[50, 55] A similar equation can be written for the desorption rate coefficient:

$$\beta_g = \frac{n_s \mathrm{H}_D k_B T d_g^3}{8 m_v D_v} \quad (5c)$$

where n_s is the vapor molecule concentration at the particle surface and H_D is the desorption rate collision kernel coefficient. These functional forms are adapted from those proposed by Ouyang et al,[55] and in them the influence of potential interactions on the collisions (but not on desporption) is considered. Rigorously, these relationships apply for circumstances in which the vapor molecule is substantially more massive than the background gas molecules. Although this is clearly not the case for water vapor molecules in air, most theoretical studies suggest that deviations from the equations presented here brought about by low mass vapor molecules are minimal.[53] Both H_S and H_D are dependent on appropriately defined diffusive Knudsen numbers (Kn_D)[56]:

$$\mathrm{H}_{S/D} = \frac{4\pi Kn_D^2 + C_1 Kn_D^3 + (8\pi)^{1/2} C_2 Kn_D^4}{1 + C_3 Kn_D + C_4 Kn_D^2 + C_2 Kn_D^3} \quad (6a)$$

where C_1 =25.836, C_2 = 11.211, C_3 = 3.502, and C_4 = 7.211. For sorption, the diffusive Knudsen number is expressed as:

$$Kn_{D,S} = \left(\frac{m_v}{k_B T}\right)^{1/2} \frac{2 D_v \eta_C}{(d_{g-1} + d_v)\eta_{FM}} \quad (6b)$$

which again considers the influence of potential interactions on collisions. For desorption, neglecting potential interactions, the diffusive Knudsen number is defined as:

$$Kn_{D,D} = \left(\frac{m_v}{k_B T}\right)^{1/2} \frac{2 D_v}{d_g} \quad (6c)$$

Enhancement factors (η_C and η_{FM}) are determined for the ion-dipole potential using the method of Fuchs[57] for the continuum regime and using kinetic theory relationships[55, 58, 59] for the free molecular regime, with the approximation that the water dipole is "locked" in alignment during its migration to a particle. This approximation, though it considerably simplifies the analysis, can lead to overestimation of the collision kernel.[59] Comparison to experimental results are hence made both considering and neglecting ion-dipole potential influences (for the latter $\eta_C = \eta_{FM} = 1$). This is discussed in greater detail in the supplementary information, which also contains tabulated values of the enhancement factors.

In classical approaches, the vapor molecule concentration at a nanoparticle surface is commonly expressed in terms of the vapor pressure over a flat liquid surface, n_{sat}, as:

$$\frac{n_s}{n_{sat}} = \exp\left(\frac{-\Delta E}{k_B T}\right) \tag{7a}$$

where ΔE is the change in free energy upon desorption of vapor molecule. A number of functional forms[6, 11, 23] have been proposed for ΔE, which can give rise to drastically different expected degrees of heterogeneous uptake for nanoparticles. ΔE values for comparison to measurements can additionally be extracted via the methods of computational chemistry.[17] For simplicity, we elect to test the combined Kelvin-Thomson-Raoult (KTR, classical theory) functional form for a singly charged particle, expressed as:

$$\Delta E = -\gamma \frac{\partial A_g}{\partial g} - \frac{e^2}{4\pi\varepsilon_0}\left(1 - \frac{1}{\varepsilon_r}\right)\frac{\partial\left(\frac{1}{d_g}\right)}{\partial g} - k_B T \ln a_w \tag{7b}$$

where γ is the surface tension of the liquid-air interface, A_g is the surface area of the particle, d_g is the particle diameter, g is the number of vapor molecules bound, ε_0 is the vacuum permittivity, ε_r is the relative permittivity of water, and a_w is the water activity on the surface of the particle.

Changes in surface area and in inverse diameter are calculated for discrete changes in g assuming that particles are spheres obeying the following relationships:

$$A_g = \pi\left[\left(d_0^3 + \frac{6}{\pi} g v_m\right)\right]^{2/3} \quad (7c)$$

$$d_g = \left[\left(d_0^3 + \frac{6}{\pi} g v_m\right)\right]^{1/3} \quad (7d)$$

where v_m is the volume of a liquid phase water molecule. Water activities are evaluated assuming that that particles undergoing heterogeneous uptake are each composed of a soluble central core with an outer saturated solution phase present, until uptake leads to complete dissolution of the core. In instances where a core exists, a_w is taken to be equivalent to the previously noted $a_{w,sat}$ values, and in instances where the core is expected to be dissolved (the determination of which is described in the supplementary information), the activity is equated with the mole fraction of water in solution (Raoult's Law). Clearly, this manner of estimating the water activity is approximate; for low amounts of sorbed vapor molecules it is not necessarily appropriate to define the sorbed layer as a saturated solution, and further activities do not "jump" from saturated solution values to ideal mixture values. In defining the free energy of desorption, other researchers have also considered the influence of surface energy at the solid core-solution interface.[18, 19, 60] While the surface energy of the solid-liquid interface can significantly affect the water activity of particles, there is limited experimental data for this parameter, and it is therefore neglected here. Finally, the liquid-air interfacial surface tension is assumed to be that of bulk solution, and free of curvature dependencies.[17] Combining equations (5a-c) & (7a) leads to:

$$K'_{eq,g} = \frac{\alpha_{g-1}}{\beta_g} = S\exp\left(\frac{\Delta E}{k_B T}\right)\frac{H_S}{H_D}\left[\frac{d_{g-1}+d_v}{d_g}\right]^3 \frac{\eta_{FM}^2}{\eta_C} \quad (8a)$$

Noting that $\Delta G_g = -k_B T \ln(K'_{eq,g}) = \Delta H_g - T\Delta S_g$, where ΔG_g, ΔH_g, and ΔS_g are the changes in Gibbs free energy, enthalpy, and entropy for the reaction $n_{g-1} \rightleftharpoons n_g$, from equation (7b) and (8a) ΔH_g and ΔS_g can be defined for KTR theory as:[8]

$$\Delta H_g = \gamma \frac{\delta A_g}{\delta g} + \frac{e^2}{4\pi\varepsilon_0}\left(1 - \frac{1}{\varepsilon_r}\right)\frac{\delta\left(\frac{1}{d_g}\right)}{\delta g} \tag{8b}$$

$$\Delta S_g = k_B\left(-\ln a_w + \ln \mathrm{S} + \ln\left[\frac{\mathrm{H}_S}{\mathrm{H}_D}\right] + 3\ln\left[\frac{d_{g-1} + d_v}{d_g}\right] + 2\ln\eta_{FM} - \ln\eta_C\right) \tag{8c}$$

We note that in most circumstances wherein classical theories for heterogeneous uptake are invoked, the ratios (H_S/H_D), $(d_{g-1}+d_v)/d_g$ as well as both enhancement factors are assumed equal to unity, leading to $\Delta S_g = k_B(-\ln a_w + \ln S)$. The inclusion of these terms here is akin to relaxing the assumptions $d_g >> d_v$ and that ion-vapor molecule potential interactions negligibly influence the collision rate.

At equilibrium, the concentration of particles with g vapor molecules sorbed, relative to the concentration which have no bound vapor molecules is expressed as:[61]

$$\frac{n_g}{n_0} = \prod_{i=1}^{g} K'_{eq,i} \tag{9a}$$

With equation (9a), the probability (P_g) that a random selected nanoparticle has g vapor molecules sorbed is:

$$P_g = \frac{n_g}{n_0 + \sum_{j=1}^{\infty} n_j} = \frac{\prod_{i=1}^{g} K'_{eq,i}}{1 + \sum_{j=1}^{\infty}\prod_{i=1}^{j} K'_{eq,i}} \qquad \text{for } g > 0 \tag{9b}$$

$$P_g = \frac{n_0}{n_0 + \sum_{j=1}^{\infty} n_j} = \frac{1}{1 + \sum_{j=1}^{\infty}\prod_{i=1}^{j} K'_{eq,i}} \qquad \text{for } g = 0 \tag{9c}$$

Noting the ergodicity of systems in equilibrium, P_g is additionally the fraction of time each nanoparticle spends within the drift tube with g sorbed vapor molecules (i.e. each nanoparticle

probes the equilibrium distribution of sorbed vapor molecules). Therefore, the average electrical mobility inferred from measurements of monomobile particles at a prescribed vapor concentration is equal to:

$$Z_{p,RH} = \sum_{g=0}^{\infty} P_g Z_{p,g} \quad (10a)$$

where $Z_{p,g}$ is the electrical mobility of a nanoparticle specifically with g sorbed vapor molecules. Correspondingly, the ratio of the electrical mobility measured at a prescribed relative humidity to the electrical mobility of nanoparticles in the absence of vapor molecules ($Z_{p,0}$) is expressed as:

$$\frac{Z_{p,RH}}{Z_{p,0}} = \sum_{g=0}^{\infty} P_g \left(\frac{Z_{p,g}}{Z_{p,0}}\right) = \frac{1+\sum_{g=1}^{\infty}\left(\left(\frac{Z_{p,g}}{Z_{p,0}}\right)\prod_{i=1}^{g} K'_{eq,i}\right)}{1+\sum_{j=1}^{\infty}\left(\prod_{i=1}^{j} K'_{eq,i}\right)} \quad (10b)$$

For approximately spherical particles, $Z_{p,RH}/Z_{p,0}$ in the free molecular limit is approximately equal to $(GF)_{RH}^{-2}$, and combining equations (2) and (10b) yields:

$$(GF)_{RH} = \left(\frac{1+\sum_{j=1}^{\infty}\left(\prod_{i=1}^{j} K'_{eq,i}\right)}{1+\sum_{g=1}^{\infty}\left(\left(\frac{d_0+d_{air}}{d_g+d_{air}}\right)^2 \prod_{i=1}^{g} K'_{eq,i}\right)}\right)^{1/2} \quad (10c)$$

When the introduction of vapor molecules negligibly influences background gas properties, equations (9) & (10) are sufficiently general to enable comparison of measured growth factors to any theoretical prediction of $K'_{eq,i}$ values (i.e. they are independent of equations 5-8), and further can be employed for any measurement system in which growth factors are inferred from the electrical mobility shifts of free molecular regime spherical particles. However, measurements are limited to instances where $\prod_{i=1}^{g} K'_{eq,i} \to 0$ as $g \to \infty$; otherwise, particles grow without bound. For saturation ratios well below unity this criterion is typically satisfied, as the product sum of equilibrium constants is proportional to S^g. A summary of the parameters used in equation (10c)

calculations, which match those during measurements, is provided in the supplementary information.

Figure 5 displays plots of the value *GF-1* from both experiments and theoretical predictions. Instances where *GF-1* is below unity are not shown. For nearly all measurements, the inferred *GF-1* values are statistically significantly greater than the minimum detectable *GF – 1* value (~0.005). Meanwhile, at low relative humidities, predictions of *GF – 1* based upon classical models, both with and without the ion-induced dipole potential considered, are near or below the minimum detectable *GF-1*; thus, we conclude that measurements are in stark disagreement with classical theory predictions despite the fact that the actual measured growth factors differ only by several percent from classical predictions. We note that the incorporation of trace amounts ammonium acetate into particles cannot explain the large disagreement between predictions and measurements, as the ammonium acetate saturated solution activity does not differ substantially from the iodide salts examined (note the activity would need to be significantly lower to bring predictions in agreement with measurements).

As emphasized in the introduction, differences between measurements and predictions with classical theory ΔE values are expected.[8] While the results presented here are for particles in a size range rarely examined, they are qualitatively similar to previous measurement of heterogeneous uptake, in which significantly more sorption has been typically observed than is predicted at low saturation ratios.[20, 62, 63] Figure 5 also shows that theoretically-predicted GFs begin to increase rapidly at a critical saturation ratio that depends upon particle size, chemical composition, and whether potential interactions influence collisions (most evident for smaller particles). This increase corresponds to the expected onset of deliquescense.[1, 12, 28] Though not clear from Figure 5, more pronounced heterogeneous uptake at a particular RH is evident in

Figures 3a & 3b for both NaI and LiI particles, which may correspond to the onset of deliquescence, though in all instances at RHs well below the expected onset RHs.

It is also important to note that although the measured growth factors are larger than classical predictions at low relative humidities, they remain small; typically *GF-1* is of order 10^{-2}. This suggests that in all circumstances, sorbed vapor molecules do not make up a substantial fraction of the particle mass. It is plausible that vapor molecules sorbed in this circumstance bind to available "sites" on particle surfaces until the formation of a monolayer, and that sorption and desorption of these vapor molecules occurs with a near constant (*g*-independent) and negative ΔE, provided there is a large number of available sites during the early stages of uptake. However, fitting constant ΔE values via equation (10c) to measurements leads to poor agreement (shown in supplemental figure S1, using ΔE ranging from -6.25 meV to -62.5 meV), similar to that found with classical theory predictions (in which ΔE varies with particle diameter).

Overall, theoretical predictions of *GF-1* values do not agree well with DMA-DTIMS inferred *GF-1* values, promoting the need for further experimental and theoretical examination of heterogeneous uptake. Only in instances where theoretical predictions of the Gibbs free energy changes associated with the sorption of successive vapor molecules are extremely accurate will predictions and measurements agree well with one another. This is clear from the functional form of equation (10c); GFs observed via DMA-DTIMS measurement are dependent on the product sum of an exponential of these free energies. Small disparities between predicted and actual free energy changes, such as the influence of vapor molecule-ion potential interactions or improper estimates of the water activity on the particle surface, can hence substantially alter the value of *GF-1*.

CONCLUSIONS

A new measurement system for studying heterogeneous uptake of vapor molecules by nanometer scale aerosol particles is described and demonstrated for water uptake by LiI and NaCl. The system includes a high resolution differential mobility analyzer (DMA), a drift tube ion mobility spectrometer (DTIMS), and a condensation particle counter (CPC) in series. The DMA-DTIMS system facilitates examination of vapor molecule uptake by particles in the 2-10 nm size range. Several features of this instrument combination make it uniquely well suited for heterogeneous uptake measurements in comparison to its DMA-DMA or DTIMS-DTIMS counterparts. First, uncertainties in measured growth factors are near 0.5%, with the minimum detectable growth factor a strong function of sampled particle concentrations. Such uncertainties are less than what is achievable for sub-10 nm particles with two conventional (resolving powers $\leq$ 10) DMAs operated in tandem[25]. Second, while higher sheath flowrate DMAs operated in tandem may afford even better resolution on single measurement basis than the DMA-DTIMS system, fluctuations in the sheath flowrates of such DMAs over the course of a measurement (which are likely, given that growth factor evaluation is more time consuming with tandem DMAs) may introduce greater measurement uncertainties, unless both DMAs are constantly recalibrated with mobility standards throughout the measurement period. Third, implementation of a DTIMS-DTIMS system for similar measurements would require more complex nanoparticle gating and data acquisition procedures than employed in the DMA-DTIMS system.

A procedure to compare measurements to theoretical predictions of the extent of heterogeneous uptake has also been presented. Measurements reveal that in the relative humidity/saturation ratio range examined, heterogeneous uptake occurs to a degree much larger than predicted by classical uptake theories. We propose that the DMA-DTIMS measurement

system will enable greater insight into the heterogeneous uptake process for small particles, particularly by making measurements at variable drift tube temperature. Such measurements will, for example, enable us to discern enthalpic from entropic influences on heterogeneous uptake. Further, we propose that the DMA-DTIMS system can be utilized not only in laboratory studies, but also in the field to study interactions between water and 2-10 nm particles formed during new particle formation events in the atmosphere.

ACKNOWLEDGEMENTS

This work was supported by National Science Foundation Grant CHE-1011810. D.R.O. acknowledges support from a National Defense Science & Engineering Graduate (NDSEG) fellowship as well as a National Science Foundation Graduate Research Fellowship (NSF GRFP). We thank Dr. Susanne Hering (Aerosol Dynamics Inc) for the loan of a WCPC 3788 for testing the prototype device.

SUPPLEMENTARY INFORMATION

A description of the procedure used to determine collision rate enhancement factors for the ion-dipole potential, determination of the number of ion-pairs present in particle cores, a list of the parameters used in predicting growth factors, and a comparison of measured growth factors to those inferred with constant ΔE are available online.

REFERENCES

1. C. Orr, F. K. Hurd and W. J. Corbett, *Journal of Colloid Science*, 1958, **13**, 472-482.
2. R. J. Weber, J. J. Marti, P. H. McMurry, F. L. Eisele, D. J. Tanner and A. Jefferson, *J Geophys Res-Atmos*, 1997, **102**, 4375-4385.
3. H. V. Nguyen and R. C. Flagan, *Langmuir*, 1991, **7**, 1807-1814.
4. S. T. Martin, G. Biskos and P. R. Buseck, *Journal of Aerosol Science*, 2009, **40**, 338-347.
5. J. J. Thomson, *Conduction of electricity through gases*, Dover Publications, New York,, 1906.
6. W. Thomson, *Proceedings of the Royal Society of Edinburgh*, 1870, **7**.
7. P. M. Winkler, G. Steiner, A. Vrtala, H. Vehkamaki, M. Noppel, K. E. J. Lehtinen, G. P. Reischl, P. E. Wagner and M. Kulmala, *Science*, 2008, **319**, 1374-1377.
8. A. W. Castleman, P. M. Holland and R. G. Keesee, *J Chem Phys*, 1978, **68**, 1760-1767.
9. I. Dzidic and P. Kebarle, *The Journal of Physical Chemistry*, 1970, **74**, 1466-1474.
10. P. M. Winkler, A. Vrtala, G. Steiner, D. Wimmer, H. Vehkamaki, K. E. J. Lehtinen, G. P. Reischl, M. Kulmala and P. E. Wagner, *Phys Rev Lett*, 2012, **108**, 085701.
11. P. Mirabel, H. Reiss and R. K. Bowles, *J Chem Phys*, 2000, **113**, 8200-8205.
12. G. Biskos, A. Malinowski, L. M. Russell, P. R. Buseck and S. T. Martin, *Aerosol Science and Technology*, 2006, **40**, 97-106.
13. H. Kohler, *Transactions of the Faraday Society*, 1936, **32**, 1152-1161.
14. P. Hamill, R. P. Turco, C. S. Kiang, O. B. Toon and R. C. Whitten, *Journal of Aerosol Science*, 1982, **13**, 561-585.
15. K. Iida, M. R. Stolzenburg and P. H. McMurry, *Aerosol Science and Technology*, 2009, **43**, 81-96.
16. J. Jiang, M. Chen, C. Kuang, M. Attoui and P. H. McMurry, *Aerosol Science and Technology*, 2011, **45**, 510-521.
17. S. M. Thompson, K. E. Gubbins, J. P. R. B. Walton, R. A. R. Chantry and J. S. Rowlinson, *J Chem Phys*, 1984, **81**, 530-542.
18. R. McGraw and E. R. Lewis, *J Chem Phys*, 2009, **131**, 194705.
19. A. K. Shchekin and A. I. Rusanov, *J Chem Phys*, 2008, **129**, 154116.
20. Y. S. Djikaev, R. Bowles, H. Reiss, K. Hameri, A. Laaksonen and M. Vakeva, *J Phys Chem B*, 2001, **105**, 7708-7722.
21. N. H. Fletcher, *The Journal of Chemical Physics*, 1958, **29**, 572-576.
22. C. S. Dutcher, X. L. Ge, A. S. Wexler and S. L. Clegg, *Journal of Physical Chemistry A*, 2013, **117**, 3198-3213.
23. A. Laaksonen, V. Talanquer and D. W. Oxtoby, *Annu Rev Phys Chem*, 1995, **46**, 489-524.
24. P. E. Wagner, D. Kaller, A. Vrtala, A. Lauri, M. Kulmala and A. Laaksonen, *Physical Review E*, 2003, **67**, 021605.
25. D. J. Rader and P. H. Mcmurry, *Journal of Aerosol Science*, 1986, **17**, 771-787.
26. E. Swietlicki, H. C. Hansson, K. HÄMeri, B. Svenningsson, A. Massling, G. McFiggans, P. H. McMurry, T. Petaja, P. Tunved, M. Gysel, D. Topping, E. Weingartner, U. Baltensperger, J. Rissler, A. Wiedensohler and M. Kulmala, *Tellus B*, 2008, **60**, 432-469.
27. I. N. Tang and H. R. Munkelwitz, *J. Colloid Interface Sci.*, 1984, **98**, 430-438.
28. I. N. Tang, *Journal of Aerosol Science*, 1976, **7**, 361-371.
29. E. J. Davis and A. K. Ray, *J. Colloid Interface Sci.*, 1980, **75**, 566-576.
30. A. E. Haddrell, J. F. Davies, A. Yabushita and J. P. Reid, *Journal of Physical Chemistry A*, 2012, **116**, 9941-9953.
31. J. Holm and J. T. Roberts, *Langmuir*, 2007, **23**, 11217-11224.
32. D. R. Oberreit, P. H. McMurry and C. J. Hogan, *Aerosol Science & Technology*, 2014, **48**, 108–118.

33. B. C. Bohrer, S. I. Merenbloom, S. L. Koeniger, A. E. Hilderbrand and D. E. Clemmer, *Annu Rev Anal Chem*, 2008, **1**, 293-327.
34. J. Fernandez de la Mora and J. Kozlowski, *Journal of Aerosol Science*, 2013, **57**, 45-53.
35. J. Fernandez de la Mora, L. de Juan, T. Eichler and J. Rosell, *Trac-Trend Anal Chem*, 1998, **17**, 328-339.
36. J. Fernandez-Garcia and J. Fernandez de la Mora, *Journal of the American Society for Mass Spectrometry*, 2013, **24**, 1872-1889.
37. S. Ude and J. Fernandez de la Mora, *Journal of Aerosol Science*, 2005, **36**, 1224-1237.
38. C. Larriba, C. J. Hogan, M. Attoui, R. Borrajo, J. Fernandez-Garcia and J. Fernandez de la Mora, *Aerosol Science and Technology*, 2011, **45**, 453-467.
39. C. Larriba and C. J. Hogan, *Journal of Physical Chemistry A*, 2013, **117**, 3887-3901.
40. C. J. Hogan and J. Fernandez de la Mora, *Physical Chemistry Chemical Physics*, 2009, **11**, 8079-8090.
41. H. E. Revercomb and E. A. Mason, *Analytical Chemistry*, 1975, **47**, 970-983.
42. S. V. Hering and M. R. Stolzenburg, *Aerosol Science and Technology*, 2005, **39**, 428-436.
43. S. V. Hering, M. R. Stolzenburg, F. R. Quant, D. R. Oberreit and P. B. Keady, *Aerosol Science and Technology*, 2005, **39**, 659-672.
44. A. C. MacMillan, T. M. McIntire, J. A. Freites, D. J. Tobias and S. A. Nizkorodov, *J Phys Chem B*, 2012, **116**, 11255-11265.
45. G. Kemmer and S. Keller, *Nature Protocols*, 2010, **5**, 267-281.
46. L. Greenspan, *Journal of Research, National Bureau of Standards (US), Series A, Physics and Chemistry*, 1977, **81**, 89-96.
47. S. L. Kaufman, J. W. Skogen, F. D. Dorman, F. Zarrin and K. C. Lewis, *Analytical Chemistry*, 1996, **68**, 1895-1904.
48. J. Rus, D. Moro, J. A. Sillero, J. Royuela, A. Casado, F. Estevez-Molinero and J. Fernandez de la Mora, *Int. J. Mass Spectrom.*, 2010, **298**, 30-40.
49. M. Gamero-Castano and J. Fernandez de la Mora, *Anal Chim Acta*, 2000, **406**, 67-91.
50. R. Gopalakrishnan and C. J. Hogan, *Physical Review E*, 2012, **85**, 026410.
51. R. Gopalakrishnan, M. R. Meredith, C. Larriba-Andaluz and C. J. Hogan, *Journal of Aerosol Science*, 2013, **63**, 126-145.
52. C. J. Hogan, K. M. Yun, D. R. Chen, I. W. Lenggoro, P. Biswas and K. Okuyama, *Colloid Surface A*, 2007, **311**, 67-76.
53. R. Gopalakrishnan and C. J. Hogan, *Aerosol Science and Technology*, 2011, **45**, 1499-1509.
54. R. Gopalakrishnan, T. Thajudeen and C. J. Hogan, *J Chem Phys*, 2011, **135**, 054302.
55. H. Ouyang, R. Gopalakrishnan and C. J. Hogan, *The Journal of Chemical Physics*, 2012, **137**, 064316.
56. B. E. Dahneke, in *Theory of Dispersed Multiphase Flow*, ed. R. E. Meyer, Academic Press, New York1983.
57. N. A. Fuchs, *Geofis. Pura Appl.*, 1963, **51**, 185-193.
58. J. E. Allen, *Phys. Scr.*, 1992, **45**, 497-503.
59. T. Su and M. T. Bowers, *Journal of the American Chemical Society*, 1973, **95**, 7609-7610.
60. L. M. Russell and Y. Ming, *J Chem Phys*, 2002, **116**, 311-321.
61. J. L. Katz and M. D. Donohue, in *Advances in Chemical Physics*, John Wiley & Sons, Inc.2007, pp. 137-155.
62. D. B. Curtis, C. D. Hatch, C. A. Hasenkopf, O. B. Toon, M. A. Tolbert, C. P. McKay and B. N. Khare, *Icarus*, 2008, **195**, 792-801.
63. M. E. Wise, S. T. Martin, L. M. Russell and P. R. Buseck, *Aerosol Science and Technology*, 2008, **42**, 281-294.

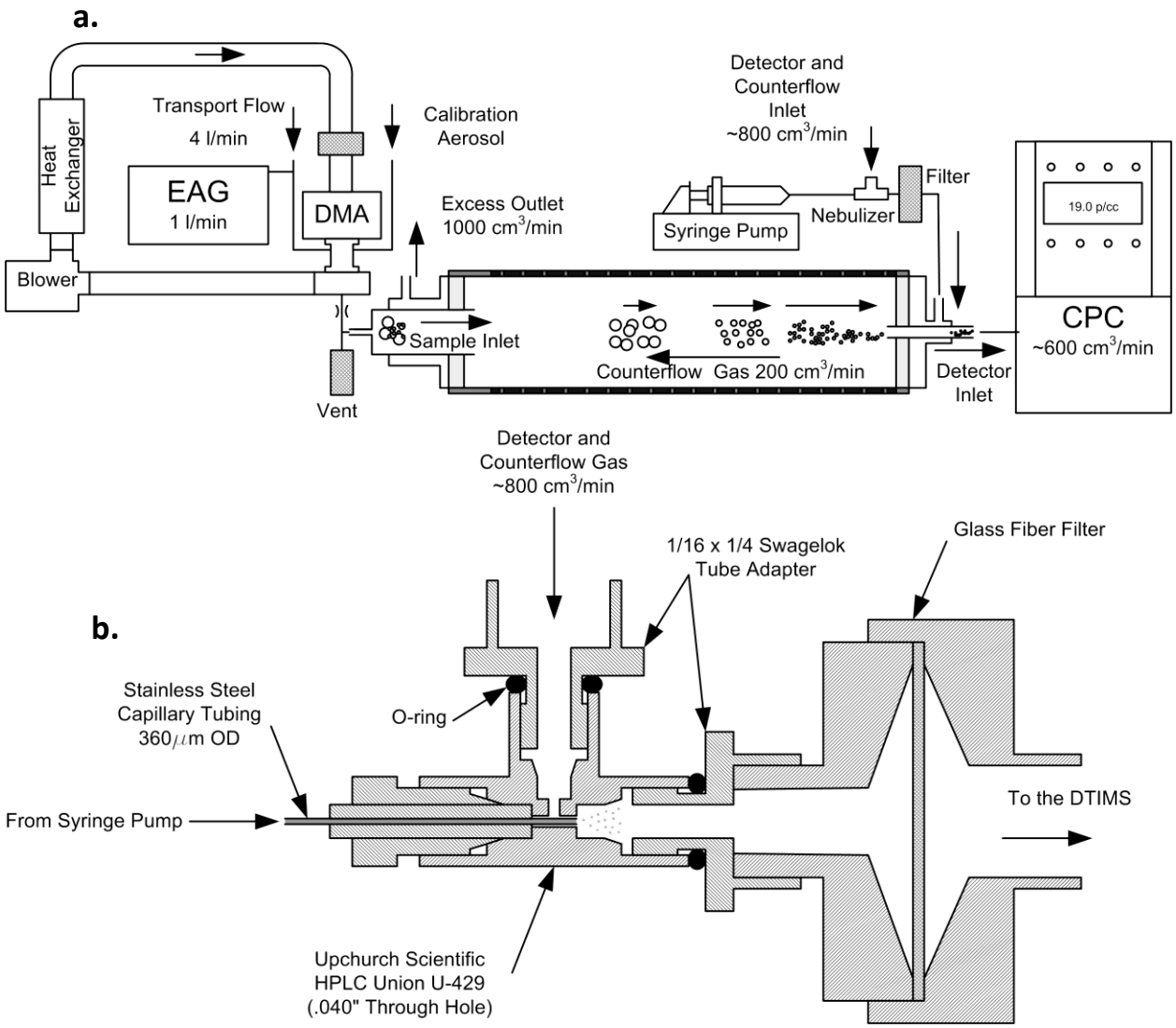

Figure 1. (a.) Schematic of the DMA-DTIMS system. EAG: Electrospray Aerosol Generator; DMA: Differential Mobility Analyzer; CPC: Condensation Particle Counter. **(b.)** Schematic of the nebulizer used to humidify the drift tube counterflow gas.

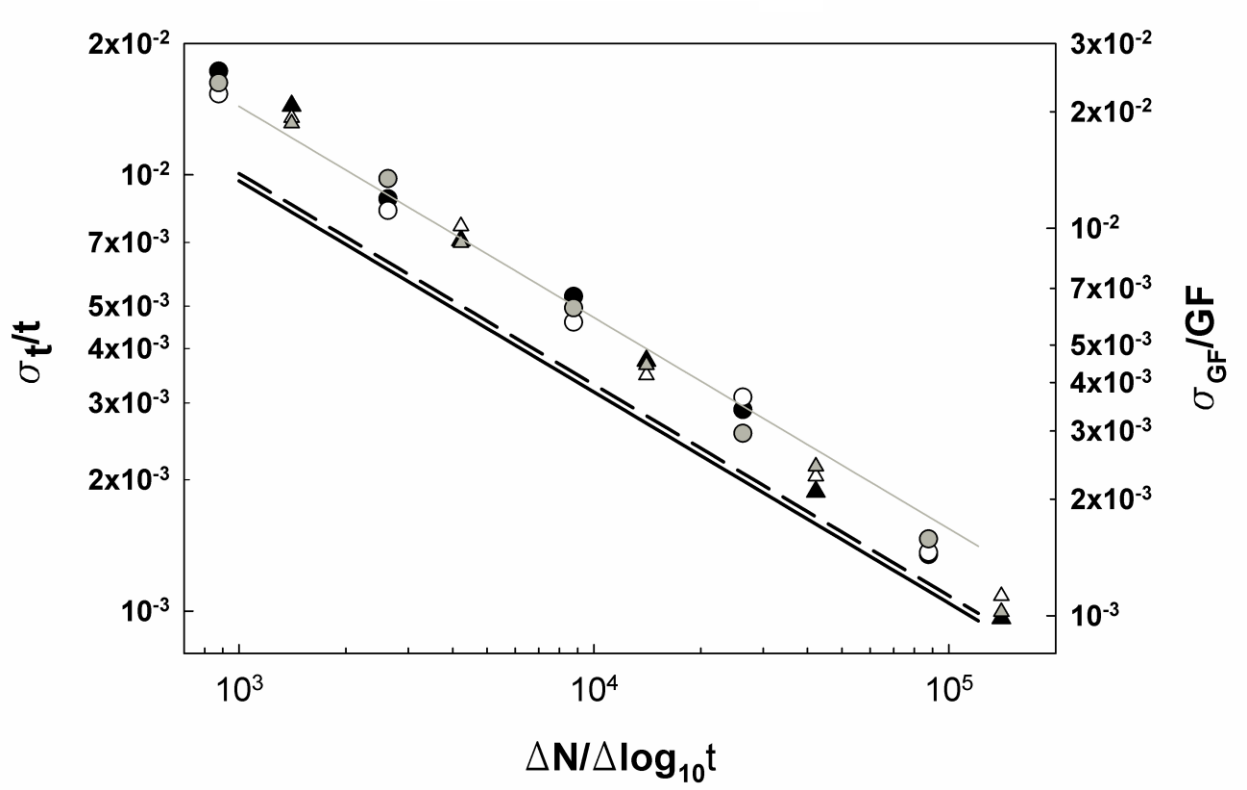

Figure 2. The arrival time standard error (symbols) for simulated DTIMS measurements and GF standard error (lines) as a function of $\Delta N/\Delta log_{10}t$, at the peak arrival time. Circles represent 150 bins per scan and triangles represent 240 bins/scan. Black symbols, peak arrival time of 1.5s; white: 2.5s; gray: 3.5s. The solid black line represents GF = 1, the dashed line is GF = 1.1, and the solid gray line is GF = 2. For the GF standard error, the value used for t_0 is 2.5s.

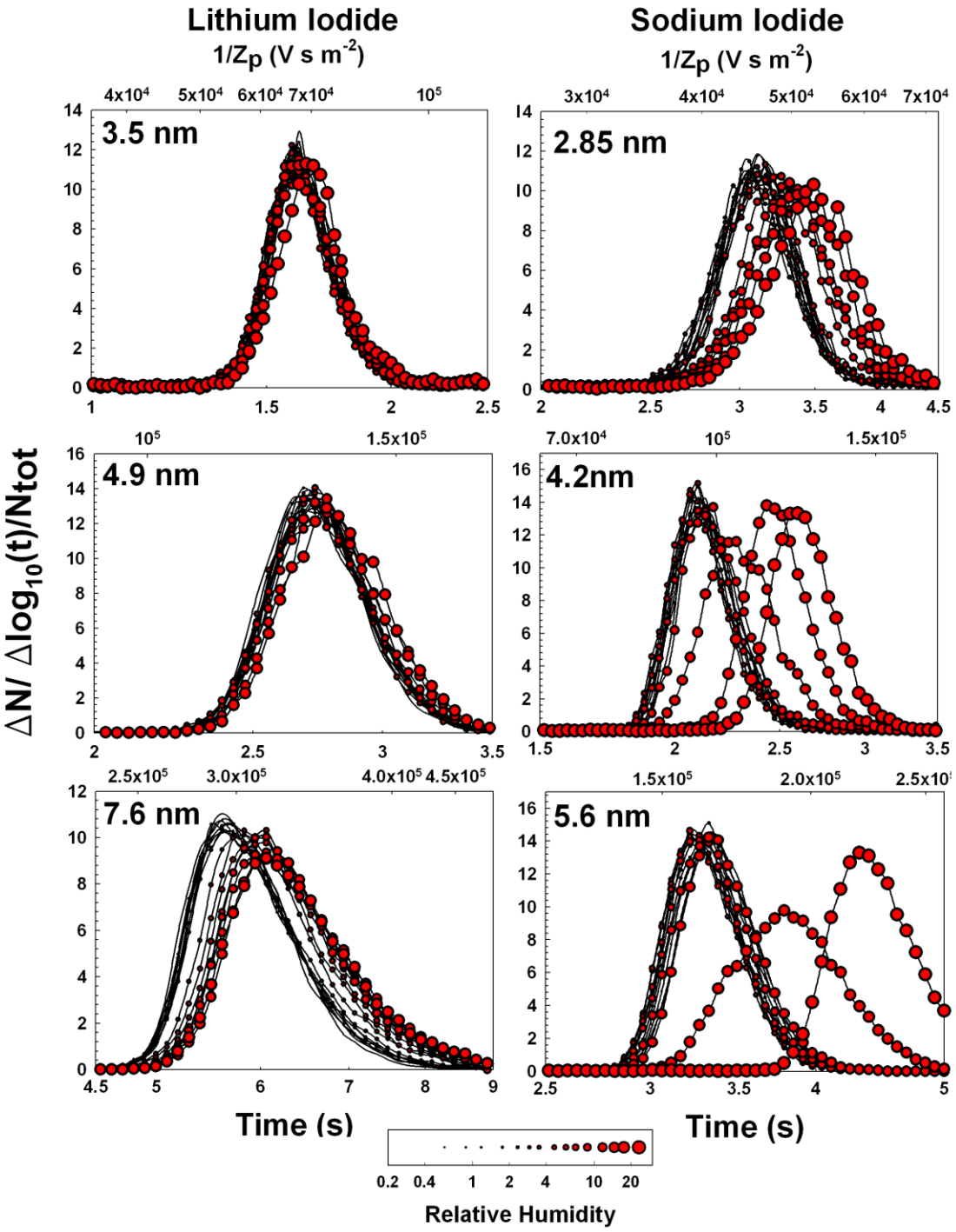

Figure 3. DMA-DTIMS arrival time distributions for lithium iodide and sodium iodide particles. The corresponding inverse electrical mobility is shown on the secondary axis for each of the distributions.

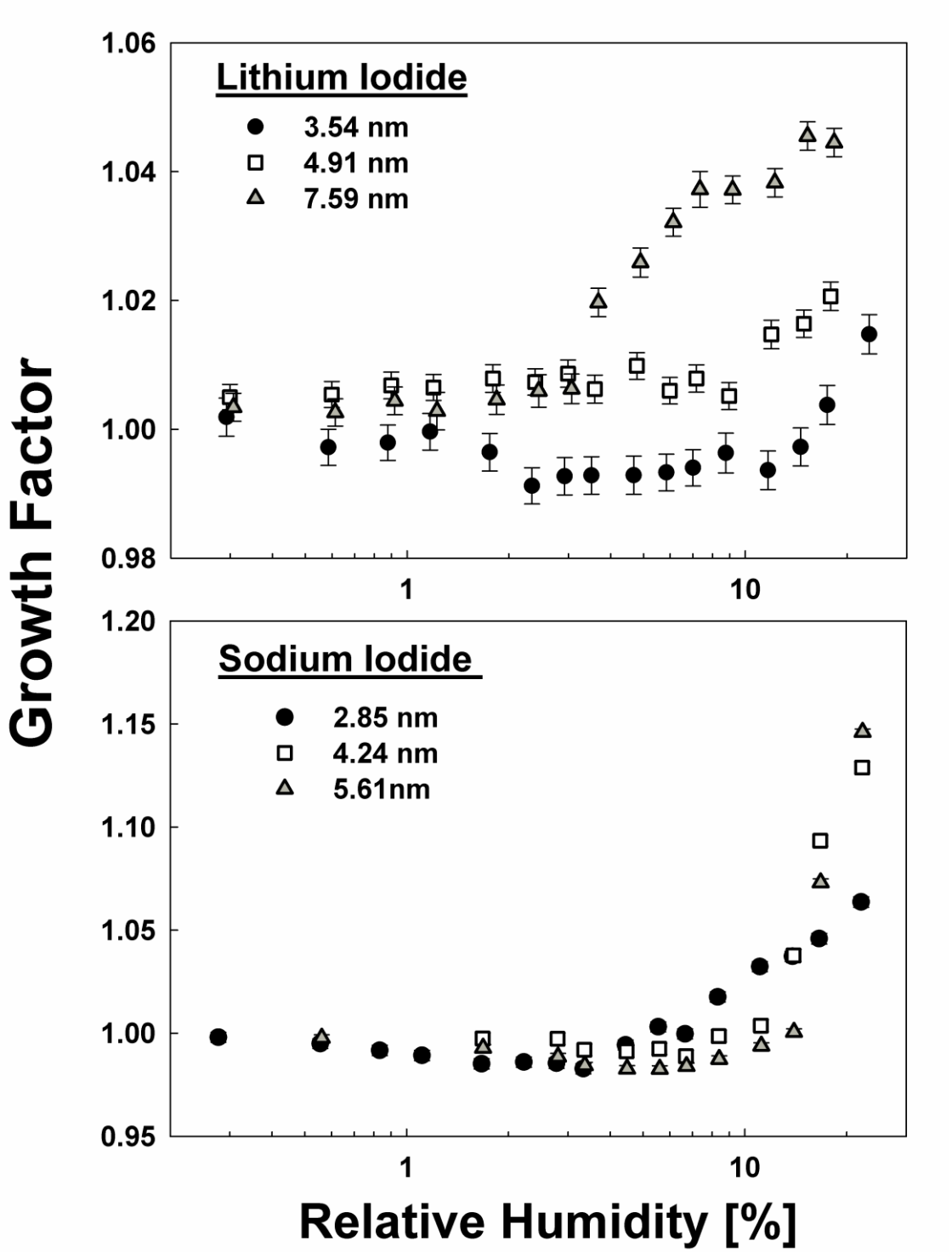

Figure 4. DMA-DTIMS inferred growth factors for **(a.)** lithium iodide and **(b.)** sodium iodide nanoparticles, measured at 23.2^{o} C and 24.2 ^{o} C respectively, as a function of the relative humidity of the drift region in the DTIMS.

5

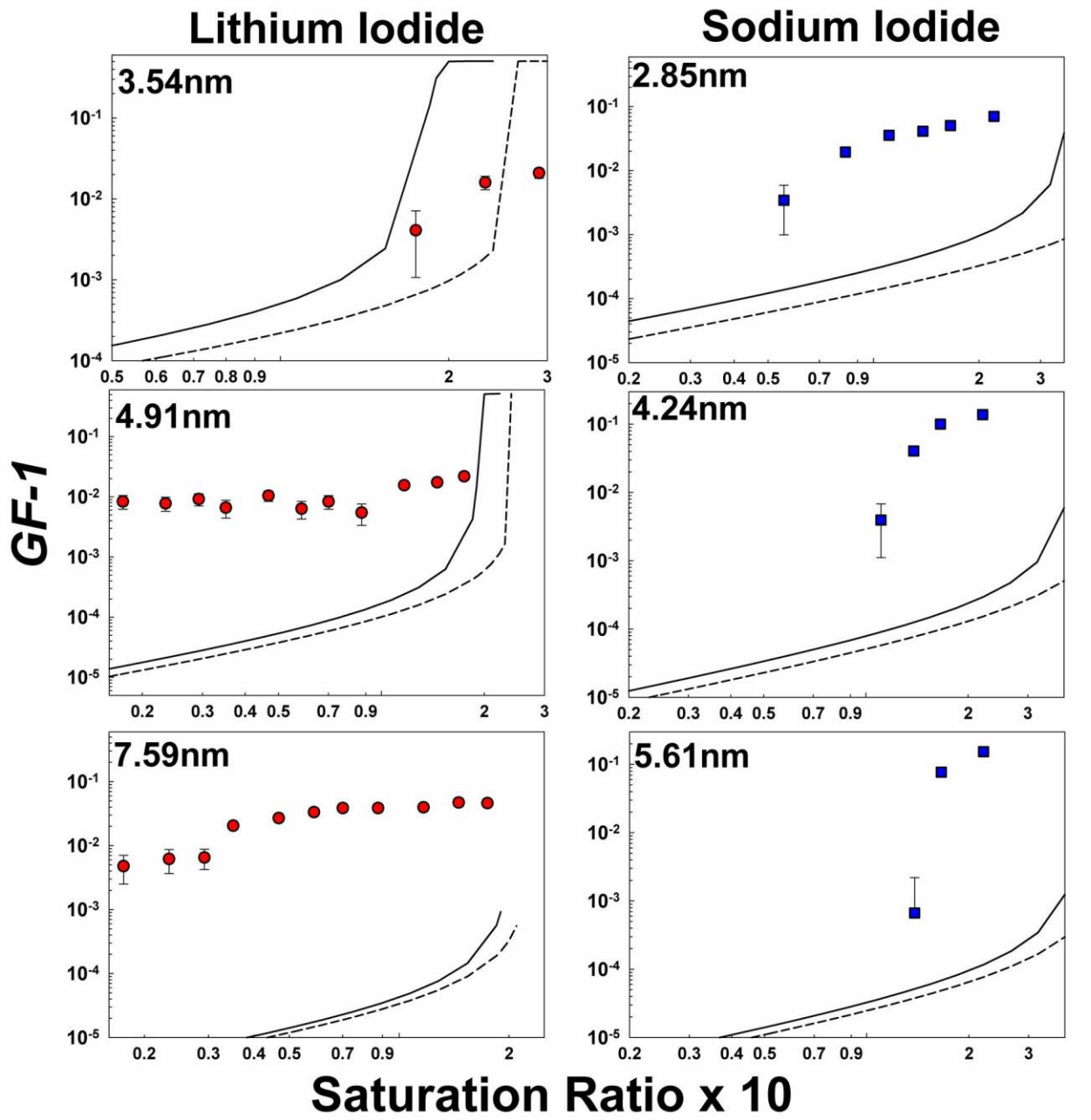

Figure 5. Comparison of measured (symbols) to theoretically predicted growth factors considering collision rate enhancement factors based on the ion-dipole potential (solid line) and collision rates calculated without potential interaction influences (dashed line).

5